



HAL
open science

Metal-insulator transition in V₂O₃ thin film caused by tip-induced strain

Natalia Alyabyeva, Joe Sakai, M. Bavencoffe, J. Wolfman, P. Limelette, H. Funakubo, A. Ruyter

► To cite this version:

Natalia Alyabyeva, Joe Sakai, M. Bavencoffe, J. Wolfman, P. Limelette, et al.. Metal-insulator transition in V₂O₃ thin film caused by tip-induced strain. Applied Physics Letters, American Institute of Physics, 2018, 113 (24), pp.241603. 10.1063/1.5063712 . hal-02014824

HAL Id: hal-02014824

<https://hal-univ-tours.archives-ouvertes.fr/hal-02014824>

Submitted on 10 Nov 2022

HAL is a multi-disciplinary open access archive for the deposit and dissemination of scientific research documents, whether they are published or not. The documents may come from teaching and research institutions in France or abroad, or from public or private research centers.

L'archive ouverte pluridisciplinaire **HAL**, est destinée au dépôt et à la diffusion de documents scientifiques de niveau recherche, publiés ou non, émanant des établissements d'enseignement et de recherche français ou étrangers, des laboratoires publics ou privés.

Metal-insulator transition in V₂O₃ thin film caused by tip-induced strain

N. Alyabyeva^{1*, a)}, J. Sakai¹, M. Bavencoffe¹, J. Wolfman¹, P. Limelette¹, H. Funakubo², and A. Ruyter¹

¹GREMAN, UMR 7347 CNRS/Université de Tours/INSA-CVL, Parc de Grandmont, 37200 Tours, France

²Tokyo Institute of Technology, 4259 Nagatsuta-cho, Midori-ku, Yokohama, 226-8502, Japan

a) Electronic mail: natalia.alabyeva@u-psud.fr

* Present address: Institut des Sciences Moléculaires d'Orsay (ISMO), CNRS, Université Paris-Saclay, F-91405 Orsay, France

ABSTRACT

We have demonstrated pressure-induced transition in a *c*-axis oriented V₂O₃ thin film from strongly correlated metal to Mott insulator in a submicrometric region by inducing a local stress using contact atomic force microscopy. To have an access to a pressure range of sub-gigapascal, a tip with a large radius of 335 nm was prepared by chemical vapour deposition of platinum onto a commercial tip with a focused ion beam (FIB). The FIB-modified tip gives a good electrical contact at low working pressures (0.25–0.4 GPa) allowing unambiguously to evidence reversible metal-insulator transition in a pulsed laser-deposited V₂O₃ thin film by means of local investigations of current-voltage characteristics. A finite element method has confirmed that the diminution of *c/a* ratio under this tip pressure explains the observed phase transition of the electron density of states in the film.

Keywords: metal-insulator transition, V₂O₃ thin films, atomic force microscopy, focused ion beam.

Vanadium sesquioxide (V_2O_3) has attracted the interest of researchers with its temperature–pressure phase diagram that consists of paramagnetic metal, paramagnetic insulator, and antiferromagnetic insulator phases, among which the switching can occur through temperature change, application of pressure or doping with another metal.^{1–4} The pure V_2O_3 , which is in the metallic phase at room temperature, is converted to the insulating phase by Cr-doping, whereas the insulating Cr-doped V_2O_3 can recover to the metallic phase under a certain hydrostatic pressure.^{1,5} It has been clarified that the c/a ratio of corundum-structured V_2O_3 -family materials significantly evolves through the phase transition. Two previous studies on the evolution of c/a ratio of (Cr-) V_2O_3 as a function of Cr-doping level¹ and as a function of hydrostatic pressure⁶ have revealed consistent behaviours to each other: insulating and metallic phases are accompanied by specific c/a regions, $c/a \leq 2.79$ for insulator and $c/a \geq 2.82$ for metal, respectively. The discontinuous change of c/a over a gap $2.79 \leq c/a \leq 2.82$ during the insulator-metal or metal-insulator phase transition gives the opportunity to induce such a transition in V_2O_3 by driving artificially its c/a to jump over this gap. It allows considering V_2O_3 as a promising material for device application based on the strain engineering. Therefore, Cr-doped V_2O_3 has been listed among candidates for the piezoresistive layer material inside piezoelectronic transistors, a perspective concept of strain-driven electronic devices.⁷

In a previous work, we have prepared a set of heteroepitaxial V_2O_3 films on C-plane sapphire [Al_2O_3 (0001)] substrates with a wide range of c/a ratio, and clarified that their c/a ratio is closely related to electrical properties.⁸ Here, we note a previous experiment that application of hydrostatic pressure to $(V_{0.96}Cr_{0.04})_2O_3$ resulted in metallization accompanied by increase (decrease) of c -(a -) axis length, thus increase of c/a ratio.¹ This suggests a picture that the c -oriented uniaxial pressure may act as if it were a negative hydrostatic pressure. Nevertheless, no study so far has been confirmed the metal-insulator transition in V_2O_3 by uniaxial pressure along any crystalline axis. Under uniform uniaxial pressure up to 0.44 GPa along c -axis, a single-crystalline V_2O_3 sample still showed metal-insulator transition during cooling at around 140 K, implying the retention of the metallic phase at room temperature.^{9,10}

The contact point at the apex of a tip is an effective medium to locally apply a huge pressure in the order of gigapascal onto a solid surface without requiring strong force. Sakai has demonstrated the local metallization of a VO_2 film grown on a metallic substrate even in a primitive point contact system with a contact area around $\sim 10 \mu m^2$.¹¹ Domingo *et al.* have used a conductive atomic force microscopy (C-AFM) with a tip radius ~ 150 nm to apply the pressure on an epitaxial Sr_2IrO_4 film and have succeeded in reducing the resistivity by five orders of magnitude with a feeble tip force of $\sim 10 \mu N$, corresponding to a pressure of ~ 10 GPa. This local metallization in Sr_2IrO_4 was attributed to a straightening of in-plane Ir–O–Ir bonding angles, as well as lattice contraction.¹²

In the present study, we have applied an external local uniaxial stress on a V_2O_3 thin film using a C-AFM in order to realize a reversible metal-insulator phase transition. On contrary to the Sr_2IrO_4 film,¹² c -axis orientation of the V_2O_3 film is expected to allow reducing its c/a ratio and driving it from metallic to insulating phase by the mean of tip pressure. For that, we have used a home-made cantilever (prepared by focused ion beam (FIB)) having a large tip radius to reach a sub-gigapascal pressure range. Results of electrical property measurements under various pressures clearly indicate a pressure-induced conductivity changes from metallic to insulator states, allowing us to evaluate the threshold pressure required for this transition.

A 82 nm thick V_2O_3 thin film was prepared on a 0.5 mm-thick single-crystalline C-plane sapphire [Al_2O_3 (0001)] substrate using pulsed laser deposition (PLD) in a vacuum chamber ($\sim 1 \times 10^{-7}$ mbar base pressure). Growth details of the film and its crystallinity investigation by X-ray diffraction (XRD, Bruker D8) are given in a supplementary material [Figure SM-1]. Resistivity of the V_2O_3 thin film at different temperature (10–300 K) without external pressure was measured by a four-probe method (Quantum Design, PPMS). Morphology and electric properties of the film were investigated using AFM (Omicron) under ultrahigh vacuum ($< 10^{-9}$ mbar) preventing the film from local anodic oxidation.¹³ Electronic properties of V_2O_3 film were characterized using C-AFM, by applying a bias voltage to the tip while an edge of the film surface was grounded. Schematic representation of C-AFM measurements causing a local stress on the V_2O_3 thin film induced by the tip is presented in a supplementary material [Figure SM-2(a)]. Local current-voltage characteristics and temporal evolution of current (at a bias voltage of 0.5 V) were carried out under various pressures (0.25 to 0.4 GPa and vice-versa). To have an access to such a low pressure range with a stable sample-surface interaction in contact mode (not accessible by standard cantilevers), a tip with a radius of 335 nm was prepared by modifying a commercial cantilever (Si_3N_4 with platinum (Pt) coating, 0.05 N/m spring constant and 45 nm initial tip radius) using FIB (Nova NanoLab 600, FEI) techniques: etching and chemical vapour deposition of Pt.¹⁴ Details of the tip preparation and its working pressure range are given in a supplementary material [Figure SM-2(b)]. To determine the tip pressure on the V_2O_3 thin film, force-distance AFM spectroscopy were taken at different regulation setpoints (0.08 to 1.2 V and vice-versa). Tip forces were estimated without taking adhesion contribution into account. Contact area at each regulation force was calculated assuming a spherical tip apex and using Hertz model.¹⁵⁻¹⁷ Young's modulus and Poisson's ratio of the FIB-modified tip were considered to be equal to those of Pt: 168 GPa and 0.38, respectively.¹⁸ 150 GPa and 0.33 were adopted for V_2O_3 .^{19,20}

The contact between the AFM tip and the V_2O_3 layer has been simulated thanks to COMSOL Multiphysics® FEA software, using the Acoustic Module and the MEMS Module, in order to investigate the spatial distribution of the lattice strain on the z-x plane under applied force ramps from 0 to 5.88 nN (0.291 GPa) by steps of 0.1 nN. The modelling criteria and assumptions are explained in a supplementary material.

Figure 1(a) shows XRD reciprocal space map around the (1 0 -1 10) reflection spot allowing to deduce lattice parameters of the film: $a = 4.958 \text{ \AA}$ and $c = 14.017 \text{ \AA}$, quite close to those of bulk values ($a = 4.954 \text{ \AA}$, $c = 14.008 \text{ \AA}$).²¹ The c/a ratio of this film is 2.827, which suggests that the sample is in the metallic phase at room temperature [Figure 1(b)].⁸ An AFM topographic image is shown in Figure 1(c). The roughness of the V_2O_3 thin film over $0.9 \times 0.4 \text{ \mu m}^2$ is found to be around 4 \AA [inset of Figure 1(c)], confirming the crystalline quality and homogeneity of the grown film.

Local characteristics of current (I) as a function of bias voltage (V) were measured at different tip pressures (P) from 0.25 to 0.4 GPa and vice-versa and plotted as average curves for all P with standard deviation for each I - V point, shown as error bars [supplementary material, Figure SM-3(a)]. Averaged I - V characteristics have been re-plotted as current density (J) vs. bias voltage by dividing the current by the tip-sample contact area in log-log scales [Figure 2(a)]. The electrical properties of the V_2O_3 film under the tip tend to be more insulating as P increases. This behavior is reproducible and reversible as confirmed by the current temporal evolution over 23 min at a fixed position and a

0.5 V bias voltage with tip pressures of 0.309, 0.326 and 0.343 GPa [Figure SM-3(b)]. As previously suggested, such conductivity change can originate from the shrinkage of the c -parameter while the a -parameter is stretched due to the perpendicular uniaxial pressure. As a result, the c/a ratio decreases in contrast with the reported increasing c/a ratio with hydrostatic pressure in bulk systems.¹ Therefore, whereas a Mott insulator can be driven into a metallic state by applying a hydrostatic pressure, a correlated metal can be driven into a Mott insulator by a c -oriented uniaxial pressure which acts in a way as a negative effective pressure increasing electronic correlations. This highlights two main features very likely related to the Mott metal-insulator transition. First, it appears that conducting properties are strongly suppressed by increasing pressure with a huge decrease of J of nearly two decades of magnitude between 0.270 and 0.291 GPa. In addition, ohmic (linear) and non-linear regimes are displayed by revealing a pressure dependent crossover voltage (V_{co}). As previously demonstrated,⁵ electrical conductivity is a relevant property in order to probe the Mott metal-insulator transition. Here, by dividing the current density by the voltage within ohmic regimes, the conductance (G) can be inferred and plotted in Figure 2(b) vs. pressure. The strong decrease of G illustrates then the transition from the metallic state to the Mott insulating state with a conductivity close to zero is due to the linear representation. Additionally, the vanishing behavior of G allows locating the Mott transition between 0.270 and 0.291 GPa. The V_{co} is defined as the threshold between ohmic and non-linear regimes [Figures 2(a) and 2(b)]. By increasing with pressure, V_{co} reveals an opposite behavior to G emphasizing the Mott insulating state. Whereas various mechanisms can be involved to explain such a non-linear crossovers, we note that the order of magnitude of V_{co} coincides quite well with the reported values of the Mott gap in Cr-doped vanadates which lie typically between 0.1 and 0.3 eV.¹ Since one may expect an increase of current if the applied voltage exceeds the energy gap, we suggest that the deduced V_{co} could mimic the behavior of the Mott gap. As a matter of fact, the decrease of V_{co} as a function of decreasing pressure could results from the lowering of electronic correlations that shorten the distance between upper and lower Hubbard bands, namely the Mott gap.²² Besides, it is worth mentioning that the rough linear variation of V_{co} with decreasing pressure suggests a vanishing behavior for a pressure around 0.25 GPa, significantly lower than the pressure range of the Mott transition previously defined with conductance. So, from the metallic side, the abrupt decrease of the conductance [inset of Figure 2(b)] results from the vanishing of the quasiparticle effective Fermi energy which leads to localization of charge carriers at a pressure around 0.28 GPa. From the insulating side, if one assumes a correspondence between the Mott gap and the crossover voltage as previously discussed, the vanishing like behavior of V_{co} in Figure 2(b) suggests a closure of the gap around 0.25 GPa. The fact that the energy gap could close at a lower pressure than the one associated with the vanishing of the characteristic metallic energy, implies a possible coexistence regime between both metallic and insulating phases which could leads to hysteresis as expected for such a first order transition. In addition, it means that when the metal is driven into the insulating phase an energy gap is already finite at the transition and the conductivity decreases abruptly [inset of Figure 2(b)]. These behaviors are key features of the Mott transition as expected in the frame of the dynamical mean field theory of strongly correlated electrons systems.^{5,14} Therefore, both conductance and crossover voltage pressure dependences strongly support the overall interpretation of a Mott metal-insulator transition.

The pressure-induced insulation observed in the V_2O_3 sample is in contrast to the pressure-induced metallization observed in Sr_2IrO_4 .¹² We suggest that the insulation is due to shrinkage (expansion) of c -(a -) axis along the out-of-plane (in-plane) direction of V_2O_3 with subsequent changes of the lattice constants ratio c/a inducing modifications of electron density of states and lattice degrees of freedom. It is caused by the fact that metallic phase corresponds to a “liquid” phase with a large density of holes and double occupancies while the insulating phase corresponds to a “gas” phase with a lower density of double occupancies and holes.²²⁻²⁴ In order to evaluate whether the critical pressure for the metal-insulator transition of around 0.3 GPa is reasonable or not, we have performed the finite element method (FEM) to obtain the c/a ratio distribution in the V_2O_3 layer under the tip [Figure 3]. Using the Poisson’s ratio of 0.33 for V_2O_3 , the simulation for a tip force of 5.88 nN, that corresponds to a pressure of 0.291 GPa, revealed the strain distribution in z and x directions [Figure 3(a, b)] allowing to determine c/a ratio diffusion as shown in Figure 3(c). The contact area with the tip is totally covered by a strained region with c/a of 2.825 or less. If one takes the cell parameters of $(V_{0.992}Cr_{0.008})_2O_3$ in McWhan and Remeika’s work,¹ which give the lower limit of c/a ratio for the metallic phase of around 2.825, this picture implies that the current flow between the Pt tip and the metallic V_2O_3 layer is interrupted by a non-metallic phase in V_2O_3 at this pressure, explaining the modification of I - V properties [Figure 1(b)]. Furthermore, we note anisotropic deformations in this material, as seen in the negative thermal expansion coefficient along c -axis¹ or in the larger compressibility of a -axis than c -axis under hydrostatic pressure.²⁵ The tendency is that a -axis length evolves more drastically compared to c -axis when the volume of a V_2O_3 cell is modified and this seems to be related to the steep gradient of the (a , c) plot for the series of V_2O_3 films grown on C -plane Al_2O_3 substrates.⁸ If we assume that the V_2O_3 material under the tip is deformed in a manner of this (a , c) scattering with such a gradient, which implies an exceptional value of Poisson’s ratio as 1.2, the local c/a ratio would be further lowered [Figure 1(b)]. The simulation at the same pressure assuming this Poisson’s ratio for V_2O_3 suggests that the local c/a value could reach 2.813 [Figure 3(d)], below the lower limit of the metallic phase (2.818) taken from the cell parameters evolution during the hydrostatic pressure-induced insulator-metal transition of $(V_{0.972}Cr_{0.028})_2O_3$, reported by Rodolakis *et al.*⁶

It will be impotent to mention, that to fulfil the study of the Mott insulator transition in V_2O_3 thin film other investigations as temperature dependence of conductivity in strained and in unstrained thin film are required and will be conducted in the next future. We consider that an unusual stress-strain relationship in V_2O_3 plays a role of lowering the critical pressure for the metal-insulator transition and is advantageous for physical properties modification using a feeble force in device forms.

In summary, transition from metal to Mott insulator was observed in a V_2O_3 thin film at room temperature by inducing a local stress under an AFM tip in contact mode. Usage of a cantilever with a 0.05 N/m spring constant and a large 335 nm tip radius gives access to a low pressure range of 0.25–0.4 GPa to probe the initial metallic phase of the film. Subsequent increase of the pressure above a threshold of ~ 0.29 GPa leads to the shrinkage (expansion) of c -(a -) axis that provokes a change of the lattice constants ratio (c/a) and consequently modifications of the electron density of states and the lattice degrees of freedom, inducing a transition from metallic to insulator phase. If

we consider a metal-insulator-metal structure in any piezoelectrically-driven switching devices, adopting a point contact scheme as the top electrode and a material that shows stress-induced metal-insulator transition, rather than insulator-metal one, would minimize the device power consumption. Therefore, we believe that metal-insulator phase transitions in V_2O_3 thin films under the impact of local external stress open perspectives for piezotransistor applications.

See in [supplementary material](#): (i) growth details of the V_2O_3 thin film and its crystallinity investigation by XRD; (ii) C-AFM measurement setup and details of tip preparation; (iii) criteria and assumptions of FEM modelling; (iv) I - V characteristics and temporal evolution of the current in V_2O_3 film under different tip pressure.

This work was conducted in GREMAN laboratory, University of Tours, France. We gratefully acknowledge Institut des Sciences Moléculaires d'Orsay (ISMO), CNRS, Université Paris-Saclay, Orsay, France for support and work promotion in European Conference on Surface Science (ECOSS 32), Grenoble, 28 August – 2 September 2016. The work was also partially supported by the Kazuchika Okura Memorial Foundation.

¹D. B. McWhan, and J. P. Remeika, Phys. Rev. B **2**, 3734 (1970).

²D. B. McWhan, A. Menth, J. P. Remeika, W. F. Brinkman, and T. M. Rice, Phys. Rev. B **7**, 1920 (1973).

³J.-H. Park, L. H. Tjeng, A. Tanaka, J. W. Allen, C. T. Chen, P. Metcalf, J. M. Honig, F. M. F. de Groot, and G. A. Sawatzky, Phys. Rev. B **61**, 11506 (2000).

⁴S. S. Majid, D. K. Shukla, F. Rahman, K. Gautam, R. J. Choudhary, V. G. Sathe, and D. M. Phase, Appl. Phys. Lett. **110**, 173101 (2017).

⁵P. Limelette, A. Georges, D. Jerome, P. Wzietek, P. Metcalf, and J.M. Honig, Science **302**, 89-92 (2003).

⁶F. Rodolakis, J.-P. Rueff, M. Sikora, I. Alliot, J.-P. Iti, F. Baudelet, S. Ravy, P. Wzietek, P. Hansmann, A. Toschi, M. W. Haverkort, G. Sangiovanni, K. Held, P. Metcalf, and M. Marsi, Phys. Rev. B **84**, 245113 (2011).

⁷D. M. Newns, B. G. Elmegreen, X.-H. Liu, and G. J. Martyna, MRS Bulletin **37**, 1071-1076 (2012).

⁸J. Sakai, P. Limelette, and H. Funakubo, Appl. Phys. Lett. **107**, 241901 (2015).

⁹J. Feinleib, and W. Paul, Phys. Rev. **155**, 841 (1967).

¹⁰S. Autier-Laurent, B. Mercey, D. Chippaux, P. Limelette, and Ch. Simon, Phys. Rev. B **74**, 195109 (2006).

¹¹J. Sakai, J. Appl. Phys. **104**, 073703 (2008).

¹²N. Domingo, L. López-Mir, M. Paradinas, V. Holy, J. Železný, D. Yi, S. J. Suresha, J. Liu, C. Rayan Serrao, R. Ramesh, C. Ocal, X. Martí, and G. Catalan, Nanoscale **7**, 3453 (2015).

¹³O. A. Ageev, N. I. Alyabieva, B. G. Konoplev, V. V. Polyakov, and V. A. Smirnov, Semiconductors **44**, 1703–1708 (2010).

¹⁴B. G. Konoplev, O. A. Ageev, V. A. Smirnov, A. S. Kolomiitsev, and N. I. Serbu, Rus. Microelectronics **41**, 41–50 (2012).

¹⁵H. R. Hertz, J. für die reine und angewandte Mathematik **92**, 156-171 (1882).

¹⁶W.C. Oliver, and G.M. Pharr, J. Mater. Res. **19**, 3-20 (2004).

¹⁷O. A. Ageev, N. I. Alyabieva, B. G. Konoplev, V. A. Smirnov, and V. V. Tkachuk, Adv. Mat. Research **894**, 374-378 (2014).

¹⁸P. Enghag, Encyclopedia of the elements, Industrilitterature, Stockholm 2004.

¹⁹S. V. Ovsyannikov, D. M. Trots, A. V. Kurnosov, W. Morgenroth, H. P. Liermann, and L. Dubrovinsky, J Phys. Condens Matter. **25**, 385401 (2013).

²⁰E. Abreu, S. N. Gilbert Corder, S. J. Yun, S. Wang, J. Gabriel Ramírez, K. West, J. Zhang, S. Kittiwatanakul, I. K. Schuller, J. Lu, S. A. Wolf, H.-T. Kim, M. Liu, and R. D. Averitt, Phys. Rev. B **96**, 094309 (2017).

- ²¹M. G. Vincent, K. Yvon, and J. Ashkenazi, *Acta Crystallogr.* **A36**, 808 (1980).²²A. Georges, G. Kotliar, W. Krauth, and M. J. Rozenberg, *Rev. Mod. Phys.* **68**, 13 (1996).
²³G. Kotliar, E. Lange, and M. J. Rozenberg, *Phys. Rev. Lett.* **84**, 5180 (2000).
²⁴M. J. Rozenberg, R. Chitra, and G. Kotliar, *Phys. Rev. Lett.* **83**, 3498 (1999).
²⁵Y. Sato, and S. Akimoto, *J. Appl. Phys.* **50**, 5285 (1979).

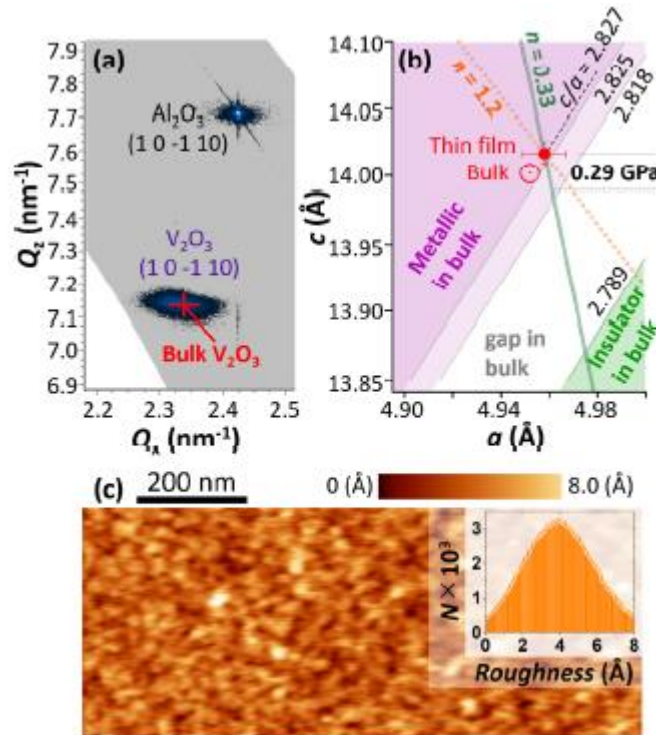


FIG. 1. (a) XRD reciprocal space map around (1 0 -1 10) reflection of the C-plane Al₂O₃ substrate and the V₂O₃ thin film. The cross represents the expected position of (1 0 -1 10) reflection from bulk V₂O₃. (b) Lattice constants (a , c) of the V₂O₃ film, as well as those of bulk V₂O₃. The c/a ratios corresponding to the border for metallic and for insulating phases in the bulk, and the lines for constant Poisson's ratios of 0.33 and 1.2 are also shown. (c) AFM topographic image of the V₂O₃ thin film and in inset the roughness distribution with N the number of events.

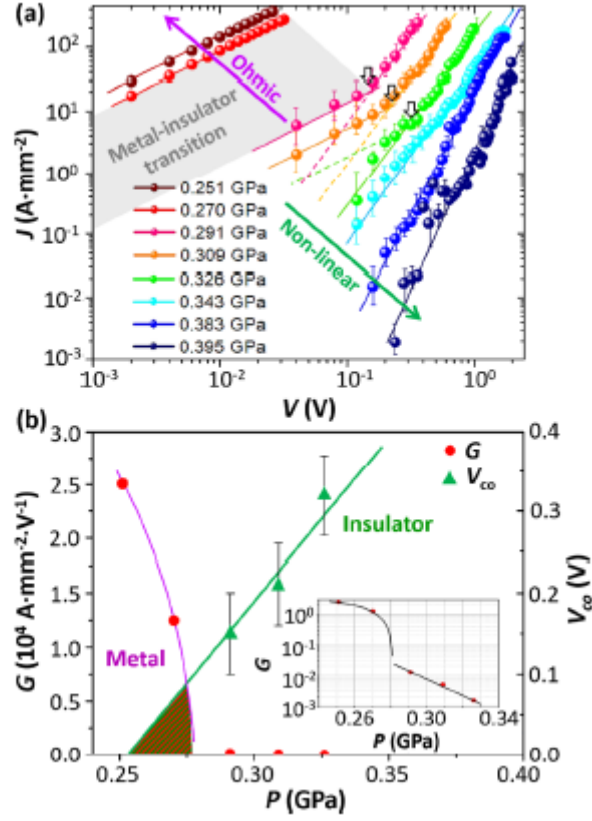


FIG. 2. (a) J vs. V characteristics under various P . Ohmic regimes are observed at $P \leq 0.326$ GPa (violet arrow), while non-linear ones at $P \geq 0.291$ GPa (green arrow). Dashed lines show slopes of regimes. Crossover points are indicated with black arrows. Metal-insulator transition is expected in a range of 0.270–0.291 GPa (grey area). (b) V_2O_3 film conductance normalized by the contact area (circle) and crossover voltage (triangle) as functions of tip pressure. Shaded area indicates possible coexistence region between metallic and insulating regimes. Inset shows conductance vs. pressure.

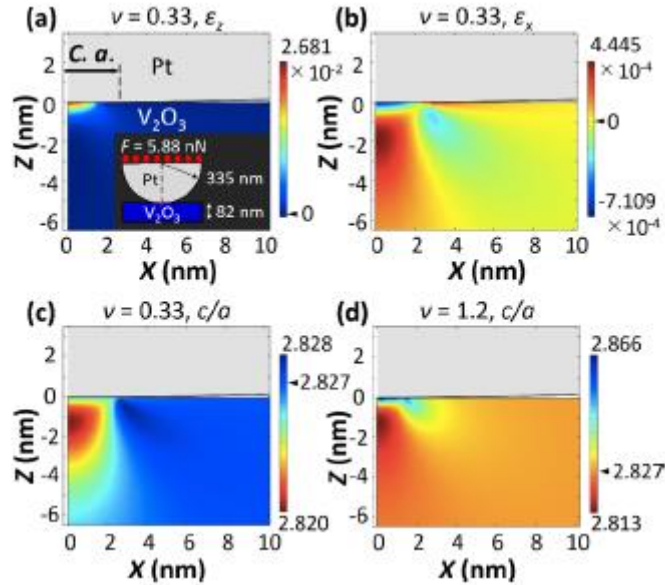


FIG. 3. (a-d) Simulated local distribution in z - x plane of strain in z (a) and x (b) directions and c/a ratio in the V_2O_3 layer assuming a Poisson's ratio for V_2O_3 of 0.33 (c) and 1.2 (d). Model of the FIB-modified Pt tip and the V_2O_3 layer for the FEM simulation in inset of (a), with $C \cdot a$ the contact area.

